# Cellulose Nanofiber Platform for Pesticide Sequestration in the Gastrointestinal Tract

Chin Guan Ho, Magdiel I. Setyawati, Glen M. DeLoid, Ke Li, Sunil S. Adav, Shuzhou Li, Say Chye Joachim Loo, Philip Demokritou, and Kee Woei Ng*

Read Online

ACCESS | Metrics & More | Article Recommendations | Supporting Information

**ABSTRACT:** Exploitation of nature-derived materials is an important approach to promote environmental sustainability. Among these materials, cellulose is of particular interest due to its abundance and relative ease of access. As a food ingredient, cellulose nanofibers (CNFs) have found interesting applications as emulsifiers and modulators of lipid digestion and absorption. In this report, we show that CNFs can also be modified to modulate the bioavailability of toxins, such as pesticides, in the gastro-intestinal tract (GIT) by forming inclusion complexes and promoting interaction with surface hydroxyl groups. CNFs were successfully functionalized with (2-hydroxypropyl)-$\beta$-cyclodextrin (HPBCD) using citric acid as a crosslinker via esterification. Functionally, the potential for pristine and functionalized CNFs (FCNFs) to interact with a model pesticide, boscalid, was tested. Based on direct interaction studies, adsorption of boscalid saturated at around 3.09% on CNFs and at 12.62% on FCNFs. Using an in vitro GIT simulation platform, the adsorption of boscalid on CNFs/FCNFs was also studied. The presence of a high-fat food model was found to have a positive effect in binding boscalid in a simulated intestinal fluid environment. In addition, FCNFs were found to have a greater effect in retarding triglyceride digestion than CNFs (61% vs 30.6%). Overall, FCNFs were demonstrated to evoke synergistic effects of reducing fat absorption and pesticide bioavailability through inclusion complex formation and the additional binding of the pesticide onto surface hydroxyl groups on HPBCD. By adopting food-compatible materials and processes for production, FCNFs have the potential to be developed into a functional food ingredient for modulating food digestion and the uptake of toxins.

Modulation of digestion by functionalized nanocellulose

## INTRODUCTION

Pesticides and fungicides, such as boscalid, are widely used in agricultural products to prevent excessive crop losses.[1] Exposure to pesticides could occur through ingestion of trace amounts of residual pesticides in food products.[2−4] Although regulations governing the maximum allowable residue levels of pesticides in food have been established, the long-term and cumulative effects of such ingestion exposures to human health are largely unknown. The uncertainties stem from the complexities in assessing real-world exposure scenarios in which ingested pesticides could interact with food compounds and the biomolecular milieu in the gastrointestinal tract (GIT) microenvironment, thereby affecting their bioavailability and subsequent effects. In our recent in vitro study, boscalid was demonstrated to interact with food additives $TiO_2$ and $SiO_2$ nanoparticles (NPs) in simulated GIT conditions, leading to its increased absorption across the intestinal barrier.[5] This emphasizes the need to understand such interactions not only to assess the fate and toxicological profiles of the ingested pesticides but also to devise strategies to modulate such

interactions and facilitate the removal of ingested pesticides from the body.

In this study, the fungicide, boscalid, was chosen as the model pesticide due to its widespread use and long-term residual stability in food products. In 2013, an EU-coordinated framework helmed by the European Food Safety Authority (EFSA) reported boscalid to be the most frequently found pesticide in all plant products,[6] and its residues were reported to be stable within the food matrices for at least 16 months.[7] Considering the high utilization rate and residual prevalence in food products, human ingestion of boscalid is a likely scenario. Hence, developing a strategy that could prevent its uptake into the human body in the GIT environment could have direct benefits in reducing health risks associated with its ingestion.

To understand the interaction of ingested boscalid with food products along the GIT microenvironment and to devise a strategy to modulate the interactions to eliminate the ingested boscalid,[8] we employed cellulose nanofibers (CNFs). Various engineered nanomaterials (ENMs) have been utilized in food products to improve the appearance and storage stability of the food products and enhance food safety and quality.[9−12] For instance, $SiO_2$ and $TiO_2$ have been used as coloring and anticaking food additives, while CNFs and other ENMs have been used in food packaging to increase shelf life and added directly to the food as a source of dietary fiber.[13−16] Recently, we demonstrated CNFs' ability as a modulator against the digestion and absorption of fat.[17] Although the exact mechanism behind this modulation has not been entirely understood, it was postulated that the combination of large surface area and highly branched networks of the CNF in suspension provided the biophysical environment to sequester fat droplets, salts, and enzymes to reduce digestion. Extending from that study, we hypothesize that CNFs could act as a platform for additional functionalization to introduce specific surface features to modulate the sequestration of pesticides such as boscalid. To test this hypothesis, we prepared functionalized CNFs (FCNFs) by introducing cyclodextrin moieties which could readily form inclusion complexes with hydrophobic molecules. Utilizing both CNFs and FCNFs, the complex interactions between nanocellulose and boscalid in the GIT, as well as fat in the food model, were investigated. Our findings showcase the enhanced performance of FCNFs as compared to CNFs in fat modulation and boscalid sequestration, highlighting their potential as a 2-in-1 dietary ingredient with both fat digestion reduction and pesticide removal functionalities.

## ■ MATERIALS AND METHODS

**CNF Production.** The nanocellulose materials were prepared as described previously.[18] In brief, CNFs were prepared through mechanical grinding with an ultrafine friction grinder (Masuko supermasscolloider small laboratory MKCA 6-2). The fibrillar materials were prepared from dried sheets NISTRM8495 (Sigma-Aldrich, Singapore) to obtain a stock concentration of 2.5% w/w cellulose.

Nanocrystalline cellulose (NCC) was produced by hydrolysis of the microcrystalline cellulose (MCC, Sigma-Aldrich Singapore), as reported elsewhere.[19] In brief, 1 g of MCC was suspended in 100 mL of a 1 M ammonium persulfate (APS, Sigma-Aldrich Singapore) solution and reacted at 60 °C for 16 h to form a white NCC suspension. After the reaction, the suspension was collected by centrifugation (22100 RCF, 10 min) and washed with DI water at least five times to completely remove the APS. Finally, the NCC pellet was lyophilized and stored in a dry box at room temperature. Both MCC and NCC were used as comparator groups in specific surface area (SSA) measurements.

**Functionalization of CNFs.** The CNF was functionalized following the previously described protocol[20,21] with minor modifications. In this method, citric acid (CA; Sigma-Aldrich, Singapore) acts as a crosslinker to graft (2-hydroxypropyl)-$\beta$-cyclodextrin (HPBCD, Sigma-Aldrich, Singapore) onto the CNF surface. In brief, HPBCD (50 mg/mL) and CA (12.5 mg/mL) were dissolved in deionized (DI) water followed by addition of 5 mg/mL of sodium phosphate monobasic dihydrate ($NaH_2PO_4$, Sigma-Aldrich, Singapore) which serves as a catalyst for the grafting process. The pristine CNF

suspension (standardized at 0.5% w/v, which was 5 mg of CNF in 1 mL) was then centrifuged at 17000 RCF for 5 min, and the excess water was decanted. 1 mL of the HPBCD/CA solution was then added into the CNF and vortexed. Functionalization was done by incubating the CNF suspension in the reaction solution at 50 °C and leaving it until it was fully dehydrated (typically 48−72 h). The dehydrated pellet was then heat-treated at 120 °C for 1 h. The functionalization process was terminated by cooling the samples at room temperature. The FCNF was then rinsed with copious water to completely remove the excess reactants, and the rinsed FCNF was then resuspended in DI water at a fixed concentration of 0.5% w/v and stored at 4 °C for further use.

**In Vitro Simulated GIT Digestion.** Whipping cream with a high fat content (35.1% w/w fat) purchased from a local supermarket was used as a heavy cream food model, while phosphate buffer (5 mM) was used as a fasting food model (FFM). Five sample groups, namely, (1) boscalid in FFM, (2) boscalid with CNFs, (3) boscalid with CNFs and cream, (4) boscalid with FCNFs, and (5) boscalid with FCNFs and cream were subjected to simulated digestions. The boscalid concentration in the tested food model was fixed at 150 ppm, the highest allowable tolerance approved by the FDA used in various food products established in Title 40 of the Code of the Federal Regulations (40 CFR §180.589). The CNF and FCNF concentrations were fixed at 0.75% w/w in the food model. The fat content in the final food model was diluted by either FFM or the CNF solution to 14% w/w of fat content.

Simplified simulated digestion was performed using a three-phase (mouth, stomach, and small intestine) simulation as previously described with slight modifications.[17] In brief, 10 mL of the food model was preconditioned to 37 °C in a water bath, mixed with 10 mL of preheated (37 °C) simulated mouth fluid (SMF, containing various salts and mucin), and incubated at 37 °C for 2 min. The oral phase digesta was added to 20 mL of simulated gastric fluid (SGF, containing salts and pepsin) and incubated at 37 °C for 2 h with mild stirring. In the small intestinal phase, the resulting gastric digesta was mixed with simulated intestinal fluid (SIF, containing salts, bile extract, and lipase). The pH was adjusted to 7, and the solution was made up to 100 mL. The incubation was resumed at 37 °C for another 2 h. For free fatty acid (FFA) quantification, the pH was maintained at pH 7.0 by titrating with a NaOH titrant, which was recorded as a function of time throughout the intestinal phase. For the quantification of pesticides, the intestinal digesta was collected at the end of the GIT simulation. The digesta was centrifuged at 17,000 RCF for 5 min, and 200 $\mu$L of the supernatant was extracted. Cold acetone (800 $\mu$L, prechilled at −20 °C) was added to the supernatant, vortexed, and further incubated at −20 °C for at least 1 h to facilitate the protein precipitation. The mixture was then centrifuged at 17,000 RCF for 5 min to collect the protein-free supernatant, which was then filtered with a 0.2 $\mu$m pore size filter and analyzed by liquid chromatography coupled with mass spectrometry (LCMS-MS) for boscalid quantification. Detection was achieved by triple quadrupole LCMS-MS Xevo TQ-S (Waters Milford, MA) with a BEH C18 column (50 mm × 2.1 mm, pore size: 1.7 $\mu$m). The column temperature was set at 30 °C, and the injection volume was 2 $\mu$L. Water with 0.1% formic acid (A) and methanol with 0.1% formic acid (B) were used as the mobile phases with gradient elution (0 min, 66% A; 2 min, 26% A; 4 min, 10% A;

5 min, 10% A; 5.1 min, 66% A; 7 min, 66% A) with a flow rate of 0.35 mL/min. The acquisition mode was multiple reaction monitoring with positive ion mode: 347.1 → 309.10 transition was used for identification (a cone voltage of 16 V and a collision energy of 32 V), while 347.1 → 141.98 was used for quantification (cone voltage at 16 V and collision energy at 30 V). The acquisition parameters for scan detection in the MS system were set as follows: the desolvation gas flow at 700 L/min, the nebulizer gas flow at 150 L/h, the desolvation temperature at 450 °C, the capillary voltage at 2.5 kV, and the source temperature at 150 °C.

**Transmission Electron Microscopy.** The CNF sample was diluted 1000 times and deposited on a lacey carbon transmission electron microscopy (TEM) grid (Ted Pella, INC.). The grid was then left to air-dry. TEM (JEOL 2010 HR) was used for imaging.

**Confocal Laser Scanning Microscopy.** The methylene blue (MB) adsorption was visualized by confocal laser scanning microscopy (CLSM) (FEI CorrSight). In brief, the nanocellulose sample was mixed with 10 $\mu$g/mL of MB for a few minutes before removing the nonadsorbed MB. After centrifuging, the supernatant was removed, and the sample was replenished with fresh DI water. The nanocellulose sample was vortexed, spread on a glass slide, and air-dried. The sample was then covered with a cover slip and sealed with nail polish. The samples were imaged with a 63× NA1.4 objective oil lens.

**SSA Determination.** The SSA was determined following the previously described method.[22] In brief, a predetermined concentration of MB and nanocellulose was mixed and incubated for 5 min. The solution was then filtered with a PTFE membrane filter (0.2 $\mu$m pore size), and the filtrate was collected for analysis. The collected filtrate was quantified as the unreacted MB. A reduction in MB concentration from the initial state was used to calculate the adsorption capacity ($q$), as shown in eq 1.

$$q = \frac{V(C_0 - C_t)}{m} \tag{1}$$

where $C_0$ and $C_t$ are the respective initial and final MB concentrations, $t$ is the incubation time, $V$ is the solution volume, and $m$ is the nanocellulose mass.

The adsorption kinetics of MB were studied following pseudo-first-order and pseudo-second-order mathematical models. For the pseudo-first order, the curve was plotted in $\ln(q_e - q_t)$ vs. time (min), where $q_e$ is the adsorption amount at equilibrium and $q_t$ is the adsorption amount at time $t$. In the case of the pseudo-second order, it was plotted in $t/q_t$ vs time (min).

The Langmuir isotherm adsorption model works with an assumption that a monolayer of adsorbate can be formed on a surface under isothermal conditions. A simple form of the Langmuir equation was hence derived as follows

$$\frac{C}{N} = \frac{C}{N_m} + \frac{1}{KN_m} \tag{2}$$

where $C$ is the equilibrium concentration and $N_m$ is the number of moles of MB per gram of cellulose required for a monolayer formation. The adsorption isotherm of cellulose samples was analyzed using this equation, in which $C/N$ vs $C$ was plotted to give the slope at $1/N_m$ and intercept at $1/KN_m$. The $q_{max}$ was then derived from the value of the slope $1/N_m$.

The SSA of nanocellulose samples was determined following the equation

$$SSA = \frac{q_{max} \times a_{MB} \times N_A}{MW} \tag{3}$$

where $q_{max}$ is the maximum adsorption capacity of MB on the sample, MW is the molecular weight of MB, $a_{MB}$ is the occupied surface area of the MB molecule (197.2 Å$^2$, assuming MB is lying flat on the nanocellulose surface), and $N_A$ is the Avogadro number ($6.023 \times 10^{23}$ mol$^{-1}$).

**Fourier-Transform Infrared Spectroscopy.** All spectra were collected by Fourier-transform infrared (FTIR) spectroscopy (PerkinElmer Frontier). CNF samples were mixed with potassium bromide (KBr) and pressed into a pellet with a hydraulic press. The spectrum resolution was fixed at 4 cm$^{-1}$, and the sample was scanned in the wavenumber range between 600 and 4000 cm$^{-1}$. A background scan was done and was automatically subtracted by the system.

**Determination of Functionalization Efficiency.** The grafting efficiency was indirectly determined through the measurement of unreacted HPBCD and CA in the reaction mixture following the functionalization process. In brief, at the end of the functionalization process, the supernatant was collected after centrifuging. The amount of HPBCD and CA in the supernatant was assayed as described in the following paragraphs.

The CA concentration was determined using ultrahigh-performance liquid chromatography–electrospray ionization mass spectroscopy (UPLC-ESI-MS). Detection was achieved by an Agilent 6120 Series with a Zorbax RX-C8 column (150 mm × 4.6 mm, pore size: 5 $\mu$m). The column temperature was set at 35 °C. Methanol with 0.1% formic acid (A) and water with 0.1% formic acid (B) were used as the mobile phases with gradient elution (0 min, 20% A; 5 min, 50% A; 6 min, 20% A) with a flow rate of 1 mL/min. The acquisition parameters for scan detection in the MS system were set as follows: the drying gas flow at 12 L/min, the nebulizer pressure at 45 psig, the drying gas temperature at 350 °C, the capillary voltage at negative 5500 V, and the fragmentor at 90 V. The detection was done by single-quadrupole ESI/MS with positive ion mode. The mass-to-charge ($m/z$) ratio of CA was set at 193 with an [H$^+$] adduct.

The HPBCD concentration was determined by the phenolphthalein method,[23] in which phenolphthalein forms inclusion complexes with HPBCD in a 1:1 host–guest ratio, resulting in an inverse relation between phenolphthalein absorbance and the amount of HPBCD in the solution. In brief, stock solutions of phenolphthalein (4 mM, Sigma-Aldrich) and sodium carbonate (125 mM, Sigma-Aldrich, Singapore) were prepared in ethanol and DI water, respectively. A reaction mixture was prepared by mixing the phenolphthalein solution, ethanol, and sodium carbonate solution in a 1:4:100 ratio. 10 $\mu$L of the reaction mixture was then added to the well plate followed by the addition of 90 $\mu$L of the supernatant containing HPBCD. A calibration curve was prepared by reacting the reaction mixture with a known amount of HPBCD. CA, being an acidic molecule, also altered the color and absorbance of the phenolphthalein solution. Therefore, a CA calibration curve was also done in a similar solution, with the absorbance of a known amount of CA (determined in UPLC-MS) subtracted to eliminate the interference. The absorbance of phenolphthalein was measured with a plate reader (Infinite M200) at a 552 nm wavelength.

**Phase Solubility Studies.** Phase solubility studies were performed according to the method described by Higuchi and Connors.[24] In brief, 1 mg of boscalid was added to 0.5 mL of 5% v/v ethanol. HPBCD (0.5 mL) at different concentrations (0−20 mM) was then added, and the mixture was left to react for 24 h at room temperature with agitation. Upon reaching equilibrium, the suspension was filtered through a 0.22 $\mu$m cellulose membrane filter to remove the undissolved solid, and the dissolved boscalid content was determined by LC−MS. The phase solubility profiles were obtained by plotting the solubility vs the concentration of HPBCD.

The apparent stability constant ($K_c$, also known as the formation constant, association constant, or binding constant) and complexation efficiency (CE) were calculated according to the equations

$$K_c = \frac{k(1-k)}{S_0} \qquad (4)$$

$$CE = \frac{slope}{1-slope} = \frac{[bos_t]}{[HPBCD]} = K_c \times S_0 \qquad (5)$$

where $S_0$ is the intrinsic solubility of boscalid in DI water without HPBCD, $k$ is the slope of the straight line, and $[bos_t]$ is the total boscalid solubility.

**Pesticide Binding Test.** To test the binding of the pesticide model, boscalid, onto the CNF and FCNF, the pesticide was first dissolved in ethanol. Various predetermined concentrations of boscalid were then added to 0.5% w/v of CNFs to determine the highest binding capacity. After 5 min of incubation, the suspension was filtered with a PTFE membrane filter (0.2 $\mu$m), and the filtrate was collected for LCMS-MS quantification.

**Nano-Isothermal Titration Calorimetry.** Nano-isothermal titration calorimetry (Nano-ITC) (TA Instruments) was used to measure the association constant ($K_a$) and dissociation constant ($K_d$) of the interaction between biomolecules, namely, boscalid, palmitic acid (PA), glyceryl tripalmitate (GTP), and HPBCD. In this study, all samples were prepared in 5% v/v ethanol to ensure adequate solubility while minimizing the heat of dilution. All solutions were degassed before the titrations. The biomolecule solution was loaded into the syringe and titrated into the cell containing a suspension of the ligand with incremental titration of 25 injections of 2 $\mu$L aliquots. The ligand concentration in the cell was varied to obtain desired stoichiometry. The injection interval between successive injections was fixed at 300 s to allow sufficient equilibration time. The stirring was set at 300 rpm to ensure thorough mixing. Data analysis was performed using Nano-Analyze software. The heat of dilution was subtracted from the raw data. The thermogram was integrated peak by peak and normalized per mole of the injectant to obtain a plot of enthalpy change per mole of biomolecules against the mole ratio of the biomolecule ligand.

**Molecular Dynamics Simulation.** The initial structures of functionalized cellulose, cellulose, boscalid, and water molecules were built using the Avogadro[25] software. Two systems were studied. Besides one boscalid and 50,000 water molecules, system one and system two include one functionalized cellulose and one unfunctionalized cellulose, respectively. Both simulation boxes were 22 nm × 10 nm × 10 nm and were packed using a random packing algorithm in Packmol.[26] The water model used in these simulations was

SPC/E,[27] and the SHAKE[28] algorithm was used to constrain the bond lengths and bond angles in the water molecules. After random packing, each box was equilibrated in the *NVT* ensemble for 1 ns at a temperature of 300 K, followed by 10 ns simulation in the *NPT* (300 K, 1 atm) ensemble. All the molecular dynamics (MD) simulations were carried out within the LAMMPS software package under periodic boundary conditions with a 1 fs time step using Ewald, specifically PPPM, to account for long-range electrostatics. The partial charges on the atomic sites of all the molecules for use in the MD simulations were determined using the 1.2*CM5 approach[29] which is optimized for the OPLSAA force field. The electronic structure calculations were performed at the HF/6-31G* level using the Gaussian 09 software.

**Electronic Structure Calculation.** In this work, all density functional theory (DFT) calculations were performed using the GAUSSIAN 09[30] suite of programs. The B3LYP[31] (Becke, 3-parameter, Lee−Yang−Parr) level of theory with the Grimme dispersion correction (D3)[32] was used along with the 6-31G* basis set. The initial structure was from classical MD simulation at 300 K and a pressure of 1 bar in the *NPT* (Nose−Hover thermostat and barostat) ensemble using the OPLSAA[33] force field. The optimized geometrical structure obtained by DFT calculation is presented in the Results and Discussion section. The binding energy was calculated using eq 6. The independent gradient model based on Hirshfeld partition (IGMH) was analyzed by the Multiwfn 3.8 program.[34]

$$E_{binding} = E_{AB} - E_A - E_B + E_{BSSE} \qquad (6)$$

**Statistical Analysis.** All quantitative data were presented as means ± standard deviation (SD). All experiments were repeated three times with $n = 3$ unless otherwise stated. Comparisons of means were done using one-way analysis of variance (ANOVA) followed by Tukey's posthoc testing with Origin data analysis software. $p < 0.05$ was considered statistically significant.

## ■ RESULTS AND DISCUSSION

**Preparation and Physicochemical and Characterization of FCNFs.** The morphology of pristine CNFs and FCNFs was analyzed using TEM, as shown in Figure 1a,b. The functionalization process yielded no notable changes in the physical appearance of CNFs as evidenced by the average fiber diameter, which remained in the range of 30.86−32.79 nm. The surface functionalization process is determined by the available surface area on CNFs for HPBCD molecules to be grafted. We therefore characterized the CNF-SSA by measuring the amount of surrogate dye MB adsorbed onto the CNF surface.[19,22,35] The adsorption of MB on CNFs was confirmed visually by CLSM. Comparison between bright-field and fluorescent images of MB-treated CNFs (Figure 1c,d) shows that MB binds homogeneously and fully adsorbs on the surface of CNFs. Accurate SSA determination hinges on the assumption that MB adsorbs onto the CNF sample as a monolayer.[22] We therefore validated the kinetics of MB interaction with CNFs (Table S1), in which a pseudo-second-order adsorption model was found to be the best fit ($R^2 > 0.99$) to describe the binding of MB onto CNFs. This indicates that MB reacted with the surface of the CNF samples by chemical sorption, instead of the more common physisorption.[19,36] The Langmuir adsorption isotherm model was noted to be a good model to describe the adsorption of MB onto
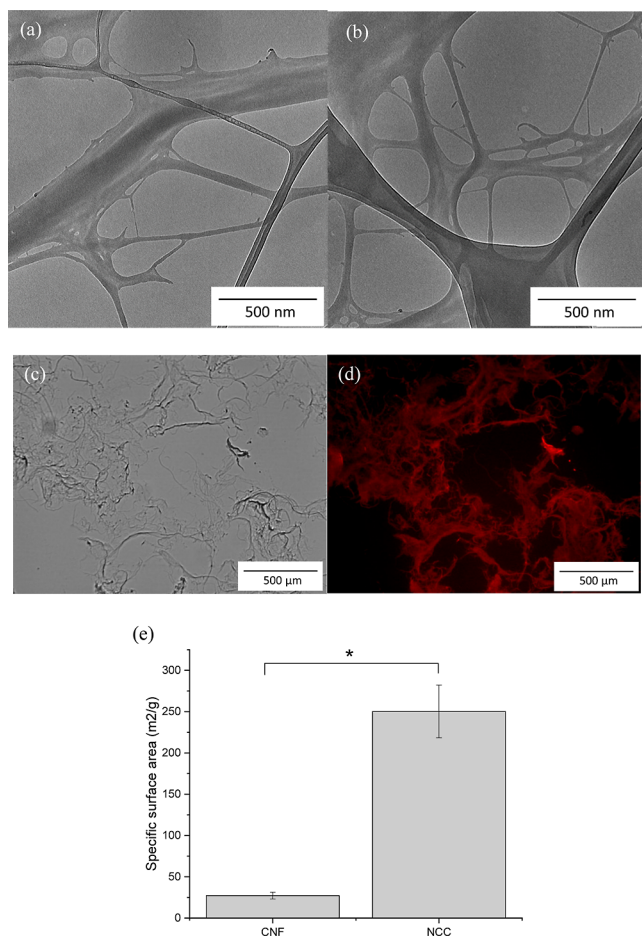
**Figure 1.** Characterization of the CNF. Representative TEM images of the (a) CNF and (b) its corresponding FCNF comparator. Scale bar: 500 nm (magnification 15,000×). (c) Bright-field and (d) corresponding CLSM images showing MB (red) adsorption on the CNF. Scale bar: 500 $\mu$m (magnification 100×). (e) SSA measurement of the CNF group and NCC comparator group. Data are means ± SD, $n = 3$, two-tailed Student's $t$-test, *$p < 0.05$, significant between compared groups.

CNFs, as evidenced by the good approximation of the adsorption constants for CNFs ($R^2 > 0.999$; Table S2),[37] further validating the formation of an MB monolayer on the CNF.

The SSA of the CNF samples was therefore calculated based on MB adsorption (Figure 1e) and was determined to be 27.20 ± 4.08 m$^2$/g ($p > 0.05$). This result is comparable to the SSA value previously estimated by electron microscopy images based on the dimensions of the CNF (34 m$^2$/g).[17]

Cyclodextrin moieties have been demonstrated to readily form inclusion complexes with various molecules, including pesticide and fat molecules,[38] and were therefore chosen as the functional groups to be grafted onto the CNF. Functionalization of the CNF with HPBCD (Figure 2a) was facilitated by the crosslinker CA in the presence of NaH$_2$PO$_4$ as the catalyst. The reaction was initiated with the dehydration step of the CA to yield a monoanhydride intermediate which could rapidly react with the hydroxyl groups on cellulose through esterification.[39] Thereafter, a second carboxylic group of CA formed a second anhydride that reacted with a hydroxyl group on HPBCD when the temperature was increased to 120 °C.

During the optimization process, a range of temperature between 90 and 120 °C was tested. Increasing the reaction temperature was found to increase the grafting efficacy as a higher temperature provides more energy for the complete esterification process. However, the CA turned yellowish-brown, suggesting its degradation at elevated temperatures (>120 °C). Therefore, 120 °C was chosen as the optimal temperature to graft HPBCD to the CNF. The CA concentration was observed to determine the overall HPBCD binding efficiency on the CNF with a small amount of CA (an initial CA concentration of 2.5 mg/mg CNF) noted to be sufficient to confer a high grafting efficiency of HPBCD (43.78%) onto the CNF surface. Additionally, increasing the amount of HPBCD beyond 25 mg/mg CNF resulted in saturation of grafting percentage and subsequent reduction of the efficacy (data not shown). The optimum grafting condition was achieved in a heating condition of 120 °C for 1 h with an initial amount of 2.5 mg CA/mg CNF and 5 mg HPBCD/mg CNF. This optimum condition yielded a grafting density of 1.56 mg CA/mg CNF (62.5% efficiency) and 2.19 mg HPBCD/mg CNF (43.8% efficiency) as shown in Figure 2b. We noted no significant difference in grafted CA amounts in the presence or absence of the catalyst, suggesting that the catalyst did not play a major role in the formation of CA−CNF ester bonds. Similarly, mixing HPBCD with the CNF in the absence of the catalyst yielded 0.60 mg HPBCD/mg CNF, while addition of the catalyst in the reaction mixture only yielded 0.37 mg HPBCD/mg CNF grafting density. HPBCD inherently could not form a chemical bond with the hydroxyl groups on CNF; thus, the small amount of HPBCD detected on the CNF could be attributed to unspecific physical adsorption and/or interaction with the minor intrinsic carboxyl groups on the CNF. When CA reacted with HPBCD, there was a significant improvement in the grafted density of both CA (1.33 mg/mg CNF) and HPBCD (1.56 mg/mg CNF). This clearly shows that there were more hydroxyl groups from HPBCD involved in the reaction, competing with the CNF for the carboxyl groups on CA to form HPBCD−CA and CA−CNF ester bonds. Addition of the catalyst NaH$_2$PO$_4$ into the reaction mixture yielded a significant increase in the overall grafting density on the CNF for both CA (1.56 mg/mg CNF) and HPBCD (2.19 mg/mg CNF) moieties, suggesting the catalyst's role in facilitating the bond formation between HPBCD and CA.

To further validate the functionalization, chemical changes in the sample groups following the grafting process were studied by FTIR spectroscopy. All tested groups, CNF, FCNF, CNF + CA, and CNF + HBPCD, exhibited common characteristic peaks attributable to the nanocellulose material (Figure 2c).[18,40] A characteristic peak at approximately 3300 cm$^{-1}$ could be assigned to −OH stretching and intermolecular hydrogen bonding in the nanocellulose material. Other nanocellulose characteristic peaks were observed at approximately 2900 cm$^{-1}$ (corresponding to the C−H stretching vibration), 1640−1650 cm$^{-1}$ (corresponding to O−H bending of adsorbed water molecules), 1460−1410 cm$^{-1}$ (corresponding to the −CH$_2$ scissoring vibration), 1040−1060 cm$^{-1}$ (corresponding to the C−O−C pyranose ring stretching), and 900−894 cm$^{-1}$ (corresponding to the cellulosic $\beta$-glycosidic linkage). More importantly, we noted prominent peaks around 1734−1745 cm$^{-1}$ on FCNF and CA-grafted CNF (CNF + CA) samples that were absent in the pristine CNF sample. This peak corresponds to C═O stretching and is
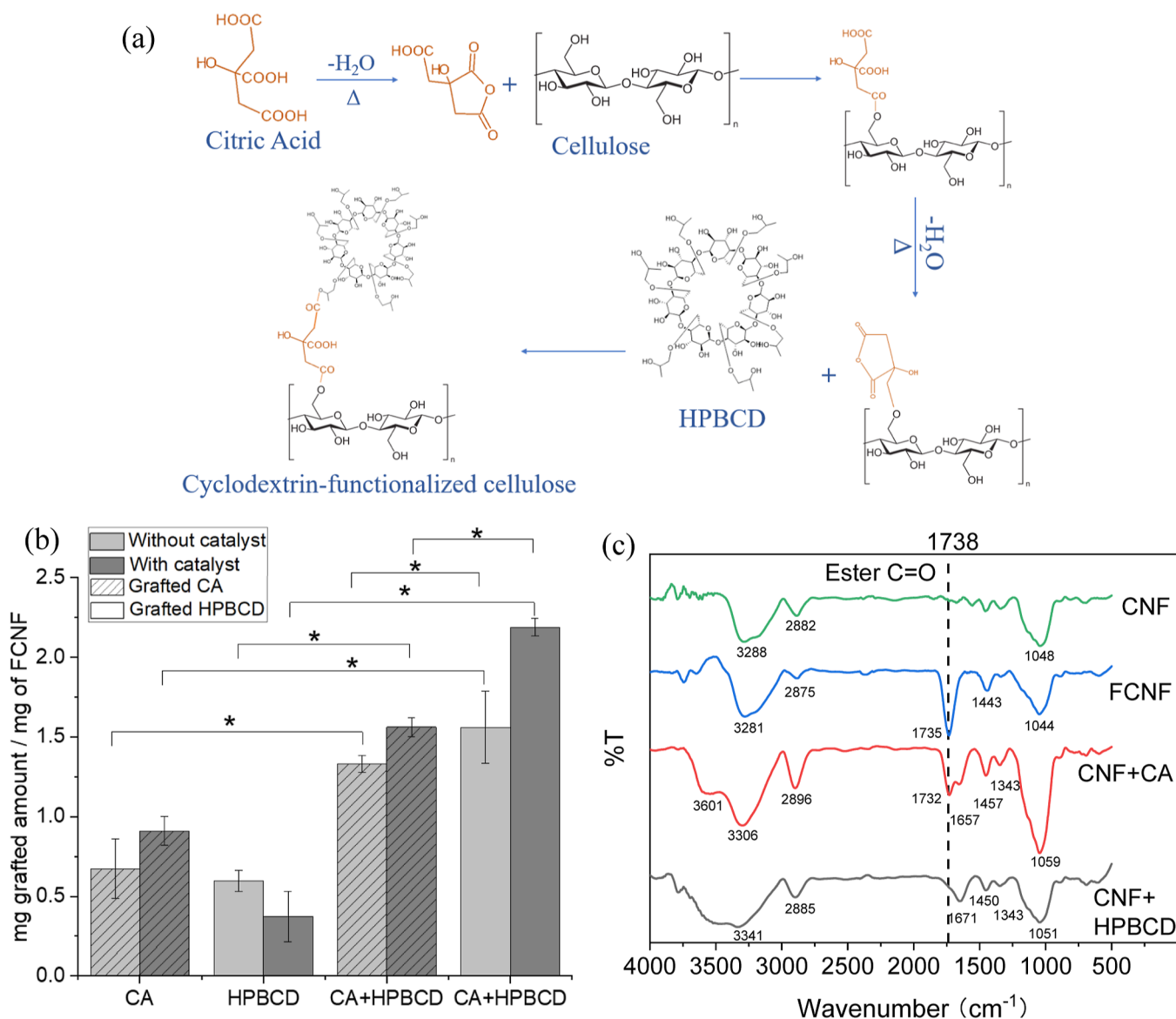
**Figure 2.** Cyclodextrin-functionalized CNF (FCNF) formation. (a) Proposed mechanism of functionalization of the CNF via esterification. (b) Amount of CA and HPBCD grafted onto the CNF across different conditions. (c) FTIR analysis indicates ester bonds resulting from the functionalization. Data are means ± SD, $n = 3$, one-way ANOVA, Tukey's HSD *posthoc* test, *$p < 0.05$, significant between compared groups.
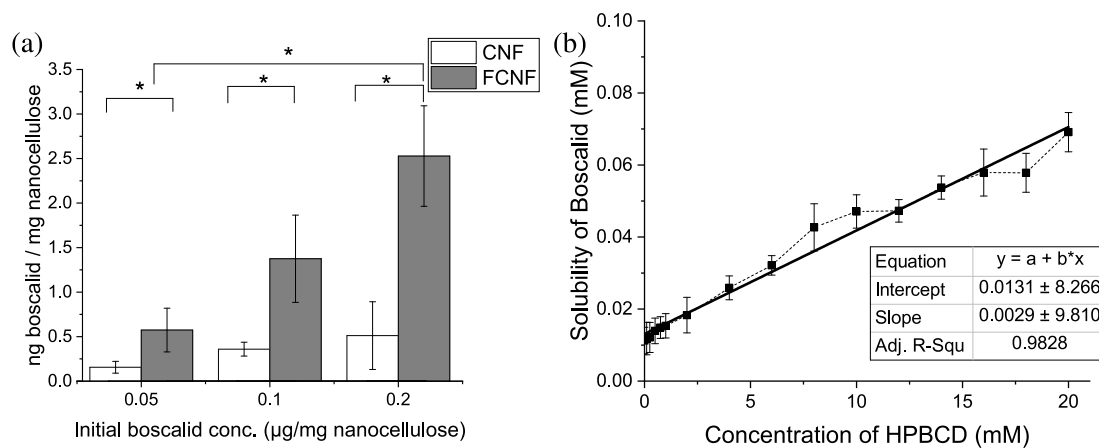


**Figure 3.** Interaction studies of boscalid. (a) Boscalid adsorption test. (b) Phase solubility diagram of boscalid vs HPBCD. Data are means ± SD, $n = 3$, one-way ANOVA, Tukey's HSD *posthoc* test, *$p < 0.05$, significant between compared groups.

attributable to the esterification process, further validating the successful functionalization of HPBCD on the CNF surface. This characteristic peak was absent in the CNF and HPBCD reaction mixture only (CNF + HPBCD), indicating no ester bonds being formed in the mixture.

**FCNF Adsorption of the Pesticide.** HPBCD is a cyclic structure that contains a large number of hydroxyl groups on its hydrophilic edges, providing the capacity to form inclusion complexes with selective small molecules. Functionalization of the CNF was facilitated by utilizing the hydroxyl groups on the CNF surface as grafting sites for the crosslinker CA and subsequently HPBCD moieties. Despite being utilized as a grafting site for HPBCD, the overall hydroxyl groups in the final FCNF are considerably higher than in the CNF due to the contribution of the hydroxyl groups from the HPBCD moieties. With multiple functionalities built-in, the FCNF therefore has the ability to interact with a multitude of biomolecules. Considering that the components including CNFs, CA, and HPBCD are all food-compatible and can be produced as food-grade materials, there is a potential to develop FCNFs into a functional platform to modulate digestion and uptake of components found in food. We therefore hypothesized that sequestration and removal of pesticides from the gut is one unmet need which this platform can address.

To test this hypothesis, we analyzed the ability of the FCNF to bind with the model pesticide, boscalid, which has been demonstrated to form inclusion complexes with cyclodextrin.[41] The adsorption study (Figure 3a) showed that both the pristine CNF and FCNF could interact and bind the model pesticide. In general, the boscalid binding capacity was observed to be significantly higher in the FCNF group (up to 4.9-fold) compared to that in the CNF. Increasing the initial boscalid concentration (0.05, 0.1, and 0.2 $\mu$g boscalid/mg nanocellulose materials) resulted in an increase in the adsorbed amount of boscalid on nanocellulose. At the tested concentration of 0.2 $\mu$g boscalid/mg nanocellulose, boscalid adsorption on the CNF and FCNF was registered to be 0.356 ng boscalid/mg and 1.95 ng boscalid/mg, respectively. Expectedly, increasing the boscalid concentration resulted in increasing amounts being sequestered onto the CNF and FCNF. This boscalid adsorbing capacity was saturated at 0.16 ng boscalid/mg CNF and 0.57 ng boscalid/mg FCNF when 0.2 $\mu$g boscalid/mg nanocellulose was used. Further addition of the CNF or FCNF into the mixture did not result in a further increase in the boscalid binding capacity of both nanocellulose samples.

To further validate the capability of the CNF and FCNF to bind to other model food components, a comparative binding analysis was also conducted using thymol (Figure S1). Thymol is a hydrophobic edible oil and has been demonstrated to interact with cyclodextrin to form inclusion complexes.[42] As with boscalid, the FCNF exhibited a significantly higher thymol binding capacity compared to the CNF. When thymol was introduced at 50 ng/mg nanocellulose, FCNF bound 71.65%, while CNF bound only 37.38% of the thymol. Further increase in the thymol concentration resulted in a decrease in the overall thymol binding efficiency, suggesting the saturation of binding sites at 19 ng thymol/mg CNF and 36 ng thymol/mg FCNF when 50 ng thymol/mg nanocellulose was used.

Comparing boscalid and thymol, the binding results show that both compounds reacted with HPBCD through different mechanisms. Inclusion complex formation between boscalid and HPBCD was less efficient because this took place through passive transport due to a concentration gradient, whereas HPBCD interaction with thymol was more active. Salvestrini et al. used an acid-activated natural clinoptilolite as an adsorbent for boscalid.[43] In contrast, they showed that the highest boscalid uptake was 0.22 mmol/kg adsorbent, which is equivalent to 76 ng boscalid/mg adsorbent. Consistent with our data, Mukherjee et al. also showed that 18% of boscalid (initial concentration of 8.54 $\mu$g/L) adsorbed onto the biomixture when the soil solution was prepared in 10 g/L; this is equivalent to 0.15 ng boscalid/mg absorbent.[44] On the other hand, Celebioglu et al. demonstrated that thymol can form an inclusion complex in 1 mg thymol/mg HPBCD,[45] which shows that thymol has higher interaction with HPBCD.

**Phase Solubility Studies.** The solubility of boscalid was plotted as a function of HPBCD concentration, as shown in Figure 3b. The observed linear relationship suggests a typical $A_L$-type profile for the boscalid-HPBCD interaction. This is attributed to the formation of 1:1 inclusion complexes between boscalid and HPBCD based on Higuchi and Connors's theory.[24] The $A_L$-type profile indicates that the solubility of one compound increased in tandem with the increasing concentration of the second compound and that only soluble complexes were formed across the concentrations tested.

The apparent stability constant, also known as the formation constant, is a measurement of the strength of the interaction between the compounds that form a complex. The calculated apparent stability constant of the boscalid/HPBCD complex was 9535.29 M$^{-1}$, indicating that boscalid has a significant tendency to enter the cavities of HPBCD. For comparison, Wang et al. reported that the apparent stability constant of *trans*-ferulic acid and HPBCD was 166.3 M$^{-1}$.[46] Stražišar et al. observed apparent stability constants for *o*-, *m*-, and *p*-coumaric acid with $\beta$-CD of 390, 2810, and 49,000 M$^{-1}$, respectively.[47] Yuan et al. determined the apparent stability constant of ethyl benzoate and HPBCD to be 9485 M$^{-1}$.[48] All of the above-mentioned investigations were based on phase solubility tests and showed that the apparent stability constant of HPBCD varied with the type of molecules. CE refers to the ratio between complex and free HPBCD, assuming 1:1 boscalid-HPBCD formation. The calculated CE was determined to be 4.55, indicating that approximately 4 out of every 5 HPBCD can form inclusion complexes with boscalid.[49] HPBCD has been proven to be a good host for inclusion complex formation, but the affinity is largely dependent on the type of guest. It is worth noting that the driving forces that facilitate inclusion complex formation are not yet fully identified;[50] thus, the interaction mechanism between boscalid and HPBCD is unclear. Several proposed mechanisms that are generally accepted include the formation of hydrogen bonds and van der Waals forces between the host and guest during complexation, a competitive replacement of water molecules from the host's cavity, and the release of the CD ring strain.[51,52] The affinity between the host and guest can also be affected by many factors including hydrophobicity, structure, size, and steric hindrance.

**In Vitro Simulated GIT Digestion.** In vitro digestion studies were conducted to simulate the conditions in the GIT. These simulations intended to demonstrate the feasibility of combining the fat-modulating ability of CNFs[17] with the pesticide binding capacity of FCNFs to reduce TG hydrolysis and prevent pesticide uptake in the GIT. Figure S2 shows the schematic of two simulated GIT studies to achieve two
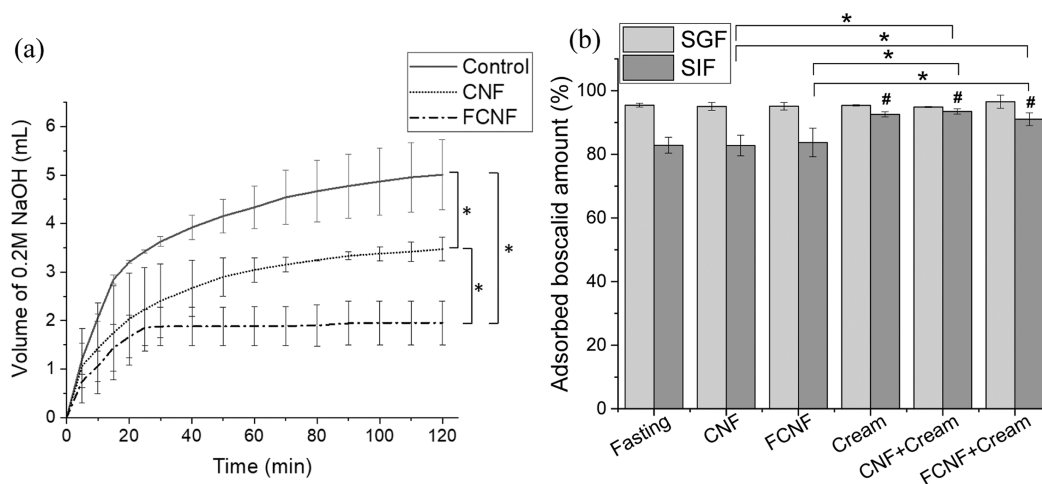
**Figure 4.** In vitro simulated GIT studies. (a) FFA quantification by pH titration. The volume of NaOH used to neutralize the mixture was proportional to the amount of FFA resulting from TG hydrolysis. Data are means ± SD, $n = 3$. Boscalid adsorption in (b) SGF and SIF environments. Data are means ± SD, $n = 3$, one-way ANOVA, Tukey's HSD *posthoc* test, $*p < 0.05$, significant between compared groups, $^\#p < 0.05$, significant against the SIF in the fasting group.

different objectives: (1) quantify the amount of adsorbed boscalid in the FCNF complex system and (2) quantify the amount of FFA to check the performance of CNFs and FCNFs in the inhibition of TG hydrolysis. The GIT is a complex environment where a plethora of substances are present in dynamic conditions, with the potential for a multitude of interactions between endogenous biomolecules and ingested materials. To date, there are no in vitro digestion systems that can fully mimic the real condition in the GIT. To generate a preliminary understanding of the binding effects of the FCNF in the GIT, a simplified simulated GIT model was adopted.[53]

The first part of the in vitro digestion study was to investigate the digestion of TG in the presence of CNFs and FCNFs. In the simulated intestinal phase digestion, TG is hydrolyzed by pancreatic lipase into FFA and glycerol. Because the formation of FFA decreases the pH in the SIF, the amount of NaOH required to neutralize the mixture is proportional to the amount of TG hydrolyzed, as shown in Figure 4a. Compared to the control group, CNFs showed significant inhibition of TG hydrolysis (30.6% reduction). CNF modulated the rheological properties of the mixture and sequestered lipid droplets, lipases, and bile salts such that they are unable to interact with each other, resulting in the reduction of TG hydrolysis. Notably, FCNFs showed an even more pronounced effect in reducing TG hydrolysis (61.0%), which plateaued after 25 min. This meant that only 39.0% of TG was converted into FFA and the rest remained as TG which would not be absorbed by the intestine. Lipid digestion is a process highly related to the interfacial properties, and the surface area of lipid droplets is critical.[54,55] Bile salts are a type of biosurfactant that can facilitate the solubilization of lipid digestion in the form of mixed micelles, which allow the lipase/colipase complex to act on the bile-coated oil droplets.[56,57] Nanocellulose disrupts the interaction between bile salt and lipid in the SIF phase, thereby reducing TG hydrolysis. Moreover, many types of materials such as pectin, guar gum, and cellulose have been explored as lipase inhibitors. Hansen observed a 12−34.8% inhibition of lipase upon addition of 12.5 g/L dietary fiber in human duodenal juice.[58] Restiawaty et al. also show that surface-modified cellulose nanocrystals can be used to immobilize lipase with a decrease in the hydrolysis

of canola oil by up to 30%.[59] Immobilization or inhibition of lipases has been a strategy used to reduce lipid digestion for the purpose of weight management. Herein, we found that functionalizing CNFs with HPBCD (FCNFs) significantly reduced the TG hydrolysis process.

The second objective of the in vitro digestion studies was to investigate pesticide adsorption in simulated GIT fluids, namely, SGF and SIF. The model pesticide, boscalid, was added to the food model (with or without cream) which then underwent subsequent modeled digestive phases. As shown in Figure S2, SGF simulation was achieved by sequentially introducing the samples through the SMF (2 min) and SGF (2 h) phases, while SIF simulation was done through the sequential introduction of the samples through the SMF (2 min), SGF (2 h), and SIF (2 h) phases. The digesta collected after passing through the SGF and SIF conditions was analyzed with LC−MS/MS separately. As described above, six conditions were tested: (1) boscalid in FFM, (2) boscalid in the FFM with CNFs, (3) boscalid in the FFM with FCNFs, (4) cream with boscalid, (5) cream with boscalid and CNFs, and (6) cream with boscalid and FCNFs. The results for SGF and SIF simulation are shown in Figure 4b.

In all samples, about 95% of boscalid was adsorbed onto components in the SGF. This was the case even in the fasting condition where no nanocellulose or food was added (control group). This showed that boscalid could interact with endogenous components present in the SGF, such as mucin and pepsin, likely due to preferential electrostatic interactions in the low-pH conditions. Consequently, there was no additional modulation effect offered by the nanocellulose platforms.

Results indicated that there was a drop in the adsorbed amount of boscalid (Figure 4a) after going through the SIF phase as compared to the SGF phase. In the fasting condition, about 83% of boscalid remained adsorbed onto various substances in the SIF, including lipase and bile salts. In the presence of cream, the amounts of boscalid adsorbed in the SIF remained comparable to those in the SGF, with close to 93% of the boscalid bound to various components in the SIF. This difference could be caused by small amounts of boscalid desorption from the pepsin in fasting conditions, while the
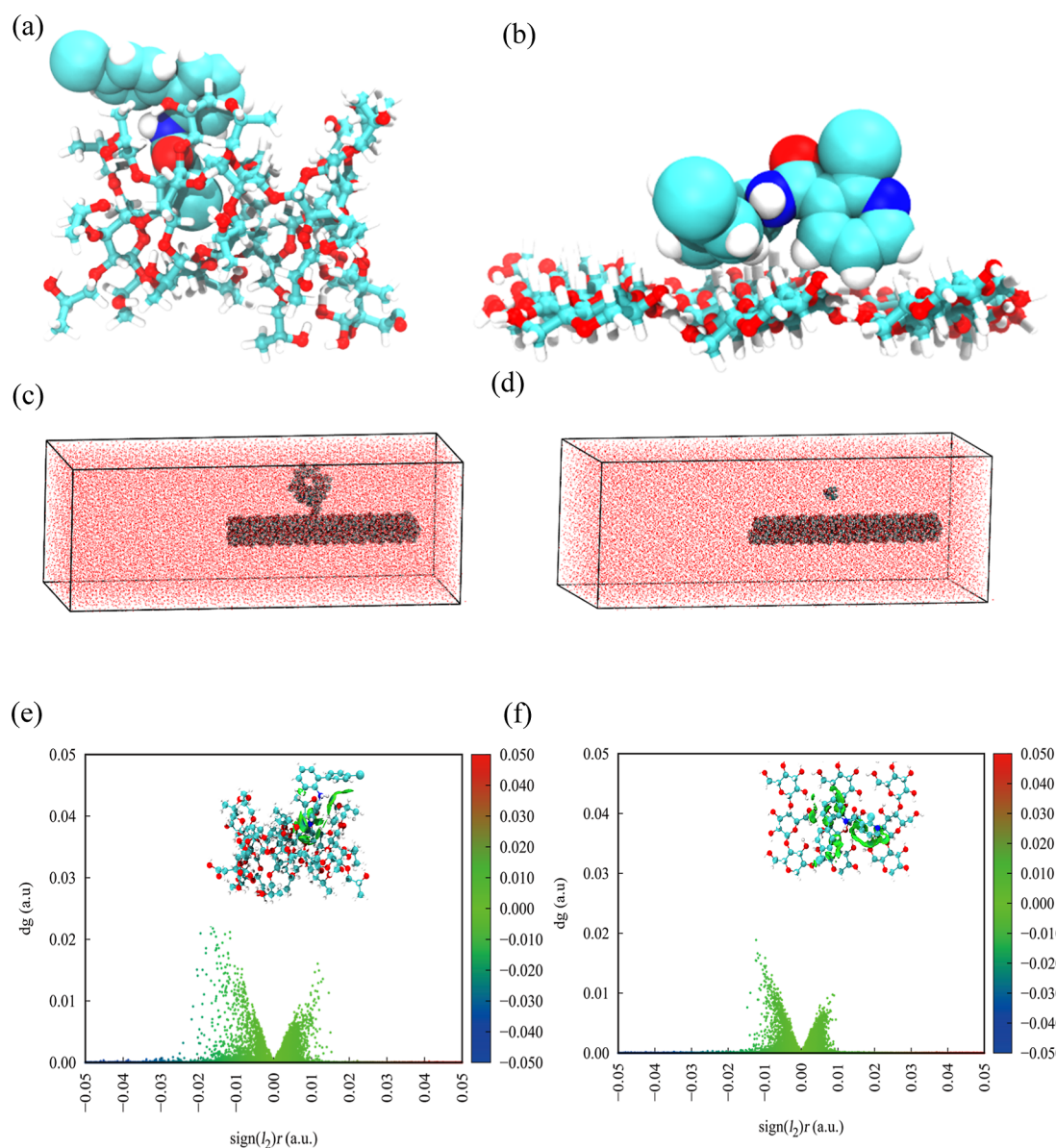
**Figure 5.** MD simulations. (a) Optimized structures for boscalid adsorbed onto HPBCD-functionalized CNFs; (b) boscalid adsorbed on the CNF surface, where carbon is in cyan, hydrogen is in white, nitrogen is in blue, and oxygen is in red. (c) System one; (d) system two, where carbon is in cyan, hydrogen is in white, nitrogen is in blue, and oxygen is in red. Red dots represent the water solvation environment. Sign$(\lambda 2)\rho$ colored scatter map between sign$(\lambda 2)\rho$ and $\delta g$inter and sign$(\lambda 2)\rho$ colored isosurfaces corresponding to IGMH analyses for (e) boscalid absorbed into the HPBCD-functionalized group; (f) boscalid absorbed on the cellulose surface, where carbon is in cyan, hydrogen is in white, nitrogen is in blue, and oxygen is in red.

boscalid that interacted with cream in SGF remained bound until the completion of digestion in the SIF. Pepsin has an isoelectric point at pH 2.7 and thus has a net negative charge in the low pH range of gastric fluid.[60] When pepsin enters the intestine with a neutral pH, it undergoes deactivation, and the protonation profile of pepsin changes. This could result in the weakening of the electrostatic interaction between boscalid and pepsin, which could potentially lead to the desorption of boscalid from pepsin as it traversed from SGF to SIF. Addition of CNFs and FCNFs did not significantly change the boscalid adsorption profile in comparison to the fasting group or the cream-alone group.

The introduction of the food model complicated the conditions in the intestinal phase. The cream mainly consists of lipids, which can be emulsified by bile salts during the intestinal digestion phase. This emulsion could form part of a corona on the cellulose surface, either as a soft corona that can be removed easily or a hard corona that persists on the nanomaterial surface.[61,62] The corona in the case of our simulated GIT model could be a combination of lipids from the cream, proteins from the enzymes, and salts present in the system. From simulated GIT results shown in Figure 4, CNFs and FCNFs in cream exhibited similar boscalid adsorption efficacies but differing results in the retardation of TG hydrolysis. DeLoid et al. suggested that nanocellulose may bridge fat droplets together to form larger clusters, thus reducing the available surface area for interaction.[17] In addition, the sequestration of bile salts by nanocellulose may change the interfacial properties of the emulsion, resulting in reduced fat digestion.[17] Nanocellulose modulates lipid

digestion, and the remaining compounds in the emulsion determine the identity of the biomolecule corona. The result in Figure 3a shows that boscalid can be adsorbed directly onto the CNF/FCNF surface, and therefore, it could also be expected to interact and become immobilized in the biomolecular corona on the surface of the CNF/FCNF. Considering that nanocellulose is indigestible, the boscalid bound to the biomolecular corona on the nanocellulose surface is expected to be excreted from the body. Compared to the CNF, the FCNF sample was noted to offer no significant advantage in removing boscalid within the tested food model system. This was possibly due to the insufficient number of inclusion complexation sites available for boscalid binding. Based on the adsorption rate of up to 3 ng boscalid/mg FCNF (Figure 3a), we estimated that less than 1 $\mu$mol of boscalid can form inclusion complexes with HPBCD grafted on the FCNF. As such, it could be expected that there would be no observable or substantial increase in adsorption when 150 $\mu$g/mL ($\sim$0.44 mM) boscalid was added to the simulated system. Nonetheless, boscalid that formed inclusion complexes with HPBCD would be expected to be excreted with the indigestible FCNF.

Considering that the CNF and FCNF possess micron scale lengths, it is unlikely for the boscalid bound on the CNF and FCNF to be transported across the GIT epithelium. A more perceivable scenario of boscalid translocation would be facilitated by its sequestration onto FFA, which was readily absorbed by the intestinal epithelium. As shown in Figure 4a, the CNF was noted to remove 30.6% of FFA, while the FCNF removed close to 61.0% of available FFA in the digesta. The efficient removal of FFA by the CNF and FCNF, together with the boscalid bound onto them, could therefore indirectly contribute to the reduction of boscalid translocation. Overall, these results suggest that the CNF and FCNF not only act as modulators of TG hydrolysis but also binders of FFA, boscalid, and boscalid-bound FFA and therefore play an essential role to reduce boscalid bioavailability in the GIT.

**Isothermal Titration Calorimetry Studies.** To further understand the interactions between the compounds in the complex GIT environment, as analyzed in the GIT simulation (i.e., boscalid, PA, GTP, and HPBCD), nano-ITC was employed. GTP was used to represent TG, whereas PA was used to represent FFA.[63,64] The dissociation constant ($K_d$) and association constant ($K_a$) of the five interactions were evaluated and are listed in Table S3. In supramolecular chemistry, it is well known that the cyclodextrin-ligand interaction has one of the lowest affinities in biology;[65–67] therefore, a sigmoidal curve in the nano-ITC thermogram for this interaction (Figure S3) could not be achieved. However, the $K_d$ can still be calculated according to the titration molar ratio (Table S3). The data was best fitted into the sequential two-site binding model with a confidence level above 95%.

Generally, the five types of interactions were in a similar order of magnitude. Their $K_d$ was in the kilomolar range ($10^3$ to $10^4$), indicating weak interactions between the tested compounds. The $K_a$ values were relatively high (less than millimolar) as compared to high-affinity antibodies which register $K_a$s in the low nanomolar ($10^{-9}$) or picomolar ($10^{-12}$) range.[68] According to the results, GTP showed relatively low interaction with both boscalid and HPBCD by registering the lowest $K_a$ values among the interaction groups. Thus, GTP was found to be the least likely to interact with boscalid and HPBCD if there was competition with other compounds.

HPBCD and boscalid were registered to have the highest interaction, followed by HPBCD and PA. It is worth noting that the abundance of compounds can also play a role in the interactions because high concentrations of one compound can dilute the interaction or reduce the contact surface of other compounds. In the simulated GIT with the cream model experiment as described in the previous section, the amounts of TG and FFA were much higher than the concentration of boscalid, which may affect the formation of inclusion complexes and the microscopic interactions with the rim of cyclodextrin.

**MD Simulations.** To further validate our experimental results, we performed MD simulations to reveal the microscale interaction mechanisms. System one studied the interaction between 1 functionalized cellulose, 1 boscalid, and 50,000 water molecules in the simulation box (22 nm × 10 nm × 10 nm), whereas system two studied 1 cellulose, 1 boscalid, and 50,000 water molecules packed into another simulation box with the same box size. From the MD simulations, we found that the boscalid molecule only adhered to the surface of the CNF surface in system two, while the boscalid molecule and the FCNF in system one formed an inclusion complex (shown in Figure 5c,d). Previous work has shown that the formation of inclusion complexes can greatly enhance the stability of small molecules.[69] Thus, boscalid is difficult to desorb from the complex, which explains why the amount of boscalid adsorbed onto the surface of the FCNF is much higher than that adsorbed onto the CNF. To further confirm this, we performed electronic structure calculations using DFT on representative clusters to compare the binding energy of a boscalid molecule with an HPBCD functional group to the binding energy of a boscalid molecule with a CNF surface. The binding energy ($\Delta E$) was calculated by eq 6, where $E_{AB}$ is the total energy of the complex with boscalid adsorbed on the FCNF surface and $E_A$ and $E_B$ are the energies of isolated boscalid and the isolated HPBCD functional group on the FCNF cluster, respectively. The binding energy between boscalid and the HPBCD-functionalized group is −33.14 kcal/mole, which is about 1.5 times larger than the binding energy between the boscalid and CNF cluster ($E$ = −21.06 kcal/mole). This result is in agreement with our experimental observations. In addition, to better understand the unbound interactions between boscalid molecules and the HPBCD functional group on the FCNF surface, the independent gradient model based on the Hirshfeld partition (IGMH) method was applied (Figure 5e,f). It clearly revealed multiple noncovalent interactions between the boscalid molecule and HPBCD functional group on the FCNF cluster. The interactions between the boscalid molecule and cellulose surface are predominated by weak van der Waals interactions (shown in green areas in Figure 5), while there are hydrogen bonds (shown in green to blue areas, Figure 5) between the boscalid molecule and HPBCD functional group.

Finally, it is worth mentioning that the studies from the authors and others on the potential toxicity of nanocellulose are evolving, and so far, such nanoscale forms of cellulose behave like micron-size cellulose which is currently considered as Generally Regarded as Safe (GRAS) by the US FDA.[70–73]

## ■ CONCLUSIONS

In this study, the CNF was successfully functionalized with HPBCD. The ability of FCNF binding and modulation capacity with lipids and boscalid was investigated. In a

simulated GIT environment, the FCNF was found to have a greater modulating effect on TG digestion compared to the CNF. Boscalid adsorption and consequent removal were increased in the presence of a high-fat food model. Nano-ITC results showed that boscalid bound more strongly to the FCNF than to the CNF. Overall, boscalid adsorbed significantly onto lipids which are in turn sequestered onto cellulose. The presence of both CNFs and FCNFs could therefore mitigate fat digestion and boscalid removal from the GIT at the same time. The FCNF has the potential to be further developed as a multipurpose food ingredient to modulate food digestion and mitigate toxin absorption into the body through the GIT.

## ■ ASSOCIATED CONTENT

### ⓢ Supporting Information

The Supporting Information is available free of charge at https://pubs.acs.org/doi/10.1021/acsomega.3c00183.

> Simulation GIT flowchart, surface area validation, and nano-ITC data (PDF)

## ■ AUTHOR INFORMATION

### Corresponding Author

Kee Woei Ng − School of Materials Science and Engineering, Nanyang Technological University, Singapore 639798, Singapore; Nanyang Environment & Water Research Institute, Singapore 637141, Singapore; ◉ orcid.org/0000-0002-7276-3563; Email: kwng@ntu.edu.sg

### Authors

Chin Guan Ho − School of Materials Science and Engineering, Nanyang Technological University, Singapore 639798, Singapore; ◉ orcid.org/0000-0003-3604-6628

Magdiel I. Setyawati − School of Materials Science and Engineering, Nanyang Technological University, Singapore 639798, Singapore

Glen M. DeLoid − Center for Nanotechnology and Nanotoxicology, Department of Environmental Health, Harvard T. H. Chan School of Public Health, Boston, Massachusetts 02115, United States; Present Address: Environmental and Occupational Health Sciences Institute, Rutgers The State University of New Jersey; ◉ orcid.org/0000-0002-6855-9172

Ke Li − Institute of Materials Research and Engineering, A*STAR (Agency for Science, Technology and Research), Singapore 138634, Singapore; ◉ orcid.org/0000-0002-3140-3983

Sunil S. Adav − School of Materials Science and Engineering, Nanyang Technological University, Singapore 639798, Singapore; ◉ orcid.org/0000-0002-8559-4885

Shuzhou Li − School of Materials Science and Engineering, Nanyang Technological University, Singapore 639798, Singapore; ◉ orcid.org/0000-0002-2159-2602

Say Chye Joachim Loo − School of Materials Science and Engineering, Nanyang Technological University, Singapore 639798, Singapore; ◉ orcid.org/0000-0001-5300-1275

Philip Demokritou − School of Materials Science and Engineering, Nanyang Technological University, Singapore 639798, Singapore; Center for Nanotechnology and Nanotoxicology, Department of Environmental Health, Harvard T. H. Chan School of Public Health, Boston, Massachusetts 02115, United States; ◉ orcid.org/0000-0002-2484-9143

Complete contact information is available at:
https://pubs.acs.org/10.1021/acsomega.3c00183

### Notes

The authors declare no competing financial interest.

## ■ ACKNOWLEDGMENTS

## ■ REFERENCES

(1) Pesticide residues in food. https://www.who.int/news-room/fact-sheets/detail/pesticide-residues-in-food (accessed 15 September 2022).

(2) Chen, X.; He, S.; Gao, Y.; Ma, Y.; Hu, J.; Liu, X. Dissipation behavior, residue distribution and dietary risk assessment of field-incurred boscalid and pyraclostrobin in grape and grape field soil via MWCNTs-based QuEChERS using an RRLC-QqQ-MS/MS technique. Food Chem. 2019, 274, 291−297.

(3) Lv, L.; Su, Y.; Dong, B.; Lu, W.; Hu, J.; Liu, X. Dissipation Residue Behaviors and Dietary Risk Assessment of Boscalid and Pyraclostrobin in Watermelon by HPLC-MS/MS. Molecules 2022, 27, 4410.

(4) Sayed, A.; Chys, M.; De Rop, J.; Goeteyn, L.; Spanoghe, P.; Sampers, I. Pesticide residues in (treated) wastewater and products of Belgian vegetable-and potato processing companies. Chemosphere 2021, 280, 130619.

(5) Cao, X.; DeLoid, G. M.; Bitounis, D.; De La Torre-Roche, R.; White, J. C.; Zhang, Z.; Ho, C. G.; Ng, K. W.; Eitzer, B. D.; Demokritou, P. Co-exposure to the food additives SiO 2 (E551) or TiO 2 (E171) and the pesticide boscalid increases cytotoxicity and bioavailability of the pesticide in a tri-culture small intestinal epithelium model: potential health implications. Environ. Sci.: Nano 2019, 6, 2786−2800.

(6) European Food Safety Authority. The 2013 European Union report on pesticide residues in food. EFSA J. 2015, 13, 4038.

(7) Anastassiadou, M.; Bernasconi, G.; Brancato, A.; Carrasco Cabrera, L.; Ferreira, L.; Greco, L.; Jarrah, S.; Kazocina, A.; Leuschner, R.; EFSA (European Food Safety Authority). Modification of the existing maximum residue level for boscalid in pomegranates. EFSA J. 2020, 18, No. e06236.

(8) Tan, S.-Y.; Wan-Yi Peh, E.; Marangoni, A. G.; Henry, C. J. Effects of liquid oil vs. oleogel co-ingested with a carbohydrate-rich meal on human blood triglycerides, glucose, insulin and appetite. Food Funct. 2017, 8, 241−249.

(9) Eleftheriadou, M.; Pyrgiotakis, G.; Demokritou, P. Nano-technology to the rescue: using nano-enabled approaches in microbiological food safety and quality. Curr. Opin. Biotechnol. 2017, 44, 87−93.

(10) Huang, R.; Vaze, N.; Soorneedi, A.; Moore, M. D.; Luo, Y.; Poverenov, E.; Rodov, V.; Demokritou, P. A novel antimicrobial technology to enhance food safety and quality of leafy vegetables using engineered water nanostructures. Environ. Sci.: Nano 2021, 8, 514−526.

(11) Huang, R.; Vaze, N.; Soorneedi, A.; Moore, M. D.; Xue, Y.; Bello, D.; Demokritou, P. Inactivation of hand hygiene-related pathogens using engineered water nanostructures. ACS Sustainable Chem. Eng. 2019, 7, 19761−19769.

(12) Vaze, N.; Pyrgiotakis, G.; Mena, L.; Baumann, R.; Demokritou, A.; Ericsson, M.; Zhang, Y.; Bello, D.; Eleftheriadou, M.; Demokritou, P. A nano-carrier platform for the targeted delivery of nature-inspired

antimicrobials using Engineered Water Nanostructures for food safety applications. *Food Control* **2019**, *96*, 365−374.

(13) Dhanyaa, M.; Devi, V. C. Nanocellulose in food packaging applications. In *AIP Conference Proceedings*; AIP Publishing LLC, 2021; p 100008.

(14) Yusoff, R.; Nguyen, L. T.; Chiew, P.; Wang, Z. M.; Ng, K. W. Comparative differences in the behavior of TiO2 and SiO2 food additives in food ingredient solutions. *J. Nanoparticle Res.* **2018**, *20*, 76.

(15) Aytac, Z.; Huang, R.; Vaze, N.; Xu, T.; Eitzer, B. D.; Krol, W.; MacQueen, L. A.; Chang, H.; Bousfield, D. W.; Chan-Park, M. B.; et al. Development of biodegradable and antimicrobial electrospun zein fibers for food packaging. *ACS Sustainable Chem. Eng.* **2020**, *8*, 15354−15365.

(16) Aytac, Z.; Xu, J.; Raman Pillai, S. K.; Eitzer, B. D.; Xu, T.; Vaze, N.; Ng, K. W.; White, J. C.; Chan-Park, M. B.; Luo, Y.; et al. Enzyme- and Relative Humidity-Responsive Antimicrobial Fibers for Active Food Packaging. *ACS Appl. Mater. Interfaces* **2021**, *13*, 50298−50308.

(17) DeLoid, G. M.; Sohal, I. S.; Lorente, L. R.; Molina, R. M.; Pyrgiotakis, G.; Stevanovic, A.; Zhang, R.; McClements, D. J.; Geitner, N. K.; Bousfield, D. W.; et al. Reducing intestinal digestion and absorption of fat using a nature-derived biopolymer: Interference of triglyceride hydrolysis by nanocellulose. *ACS Nano* **2018**, *12*, 6469−6479.

(18) Pyrgiotakis, G.; Luu, W.; Zhang, Z.; Vaze, N.; DeLoid, G.; Rubio, L.; Graham, W. A. C.; Bell, D. C.; Bousfield, D.; Demokritou, P. Development of high throughput, high precision synthesis platforms and characterization methodologies for toxicological studies of nanocellulose. *Cellulose* **2018**, *25*, 2303−2319.

(19) He, X.; Male, K. B.; Nesterenko, P. N.; Brabazon, D.; Paull, B.; Luong, J. H. Adsorption and desorption of methylene blue on porous carbon monoliths and nanocrystalline cellulose. *ACS Appl. Mater. Interfaces* **2013**, *5*, 8796−8804.

(20) Marshall, W. E.; Wartelle, L.; Boler, D.; Johns, M.; Toles, C. Enhanced metal adsorption by soybean hulls modified with citric acid. *Bioresour. Technol.* **1999**, *69*, 263−268.

(21) Thanh, N. D.; Nhung, H. L. Cellulose modified with citric acid and its absorption of Pb2+ and Cd2+ ions. *Proceedings of 13rd International Electronic Conference on Synthetic Organic Chemistry (ECSOC-13)*, 2009.

(22) Kaewprasit, C.; Hequet, E.; Abidi, N.; Gourlot, J. P. Quality measurements. *J. Cotton Sci* **1998**, *2*, 164−173.

(23) Kuwabara, T.; Takamura, M.; Matsushita, A.; Ikeda, H.; Nakamura, A.; Ueno, A.; Toda, F. Phenolphthalein-modified *β*-cyclodextrin as a molecule-responsive colorless-to-color change indicator. *J. Org. Chem.* **1998**, *63*, 8729−8735.

(24) Higuchi, T.; Connors, K. A phase solubility technique. *Adv. Anal. Chem. Instrum.* **1965**, *4*, 117−211.

(25) Hanwell, M. D.; Curtis, D. E.; Lonie, D. C.; Vandermeersch, T.; Zurek, E.; Hutchison, G. R. Avogadro: an advanced semantic chemical editor, visualization, and analysis platform. *J. Cheminf.* **2012**, *4*, 17.

(26) Martínez, L.; Andrade, R.; Birgin, E. G.; Martínez, J. M. PACKMOL: A package for building initial configurations for molecular dynamics simulations. *J. Comput. Chem.* **2009**, *30*, 2157−2164.

(27) Mark, P.; Nilsson, L. Structure and Dynamics of the TIP3P, SPC, and SPC/E Water Models at 298 K. *J. Phys. Chem. A* **2001**, *105*, 9954−9960.

(28) Kräutler, V.; van Gunsteren, W. F.; Hünenberger, P. H. A fast SHAKE algorithm to solve distance constraint equations for small molecules in molecular dynamics simulations. *J. Comput. Chem.* **2001**, *22*, 501−508.

(29) Dodda, L. S.; Vilseck, J. Z.; Tirado-Rives, J.; Jorgensen, W. L. 1.14*CM1A-LBCC: Localized Bond-Charge Corrected CM1A Charges for Condensed-Phase Simulations. *J. Phys. Chem. B* **2017**, *121*, 3864−3870.

(30) Frisch, M. J.; Trucks, G. W.; Schlegel, H. B.; Scuseria, G. E.; Robb, M. A.; Cheeseman, J. R.; Scalmani, G.; Barone, V.; Mennucci, B.; Petersson, G. A.; Nakatsuji, H.; Caricato, M.; Li, X.; Hratchian, H.

P.; Izmaylov, A. F.; Bloino, J.; Zheng, G.; Sonnenberg, J. L.; Hada, M.; Ehara, M.; Toyota, K.; Fukuda, R.; Hasegawa, J.; Ishida, M.; Nakajima, T.; Honda, Y.; Kitao, O.; Nakai, H.; Vreven, T.; Montgomery, J. A.; Peralta, J. E.; Ogliaro, F.; Bearpark, M.; Heyd, J. J.; Brothers, E.; Kudin, K. N.; Staroverov, V. N.; Kobayashi, R.; Normand, J.; Raghavachari, K.; Rendell, A.; Burant, J. C.; Iyengar, S. S.; Tomasi, J.; Cossi, M.; Rega, N.; Millam, J. M.; Klene, M.; Knox, J. E.; Cross, J. B.; Bakken, V.; Adamo, C.; Jaramillo, J.; Gomperts, R.; Stratmann, R. E.; Yazyev, O.; Austin, A. J.; Cammi, R.; Pomelli, C.; Ochterski, J. W.; Martin, R. L.; Morokuma, K.; Zakrzewski, V. G.; Voth, G. A.; Salvador, P.; Dannenberg, J. J.; Dapprich, S.; Daniels, A. D.; Farkas, Ö.; Foresman, J. B.; Ortiz, J. V.; Cioslowski, J.; Fox, D. J. *Gaussian 09*, Revision A.2; Gaussian Inc., 2009.

(31) Stephens, P. J.; Devlin, F. J.; Chabalowski, C. F.; Frisch, M. J. Ab Initio Calculation of Vibrational Absorption and Circular Dichroism Spectra Using Density Functional Force Fields. *J. Phys. Chem.* **1994**, *98*, 11623−11627.

(32) Grimme, S.; Hansen, A.; Brandenburg, J. G.; Bannwarth, C. Dispersion-Corrected Mean-Field Electronic Structure Methods. *Chem. Rev.* **2016**, *116*, 5105−5154.

(33) Jorgensen, W. L.; Maxwell, D. S.; Tirado-Rives, J. Development and Testing of the OPLS All-Atom Force Field on Conformational Energetics and Properties of Organic Liquids. *J. Am. Chem. Soc.* **1996**, *118*, 11225−11236.

(34) Lu, T.; Chen, F. Multiwfn: A multifunctional wavefunction analyzer. *J. Comput. Chem.* **2012**, *33*, 580−592.

(35) Skripkina, T.; Podgorbunskikh, E.; Bychkov, A.; Lomovsky, O. Sorption of methylene blue for studying the specific surface properties of biomass carbohydrates. *Coatings* **2020**, *10*, 1115.

(36) Ho, Y.-S.; McKay, G. Pseudo-second order model for sorption processes. *Process Biochem.* **1999**, *34*, 451−465.

(37) Elmorsi, T. M. Equilibrium isotherms and kinetic studies of removal of methylene blue dye by adsorption onto miswak leaves as a natural adsorbent. *J. Environ. Prot.* **2011**, *02*, 817−827.

(38) Cid-Samamed, A.; Rakmai, J.; Mejuto, J. C.; Simal-Gandara, J.; Astray, G. Cyclodextrins inclusion complex: Preparation methods, analytical techniques and food industry applications. *Food Chem.* **2022**, *384*, 132467.

(39) Zhou, Y.; Luner, P.; Caluwe, P. Mechanism of crosslinking of papers with polyfunctional carboxylic acids. *J. Appl. Polym. Sci.* **1995**, *58*, 1523−1534.

(40) Li, M.; He, B.; Chen, Y.; Zhao, L. Physicochemical properties of nanocellulose isolated from cotton stalk waste. *ACS Omega* **2021**, *6*, 25162−25169.

(41) Zhang, Y.; Kuang, J.; Dong, J.; Shi, L.; Li, Q.; Zhang, B.; Shi, W.; Huang, X.; Zhu, Z.; Ma, Y.; et al. Ultra-sensitive boscalid sensors based on a *β*-cyclodextrin modified perfluorinated copper phthalo-cyanine field-effect transistor. *J. Mater. Chem. C* **2021**, *9*, 12877−12883.

(42) Tao, F.; Hill, L. E.; Peng, Y.; Gomes, C. L. Synthesis and characterization of *β*-cyclodextrin inclusion complexes of thymol and thyme oil for antimicrobial delivery applications. *LWT–Food Sci. Technol.* **2014**, *59*, 247−255.

(43) Salvestrini, S.; Vanore, P.; Iovino, P.; Leone, V.; Capasso, S. Adsorption of simazine and boscalid onto acid-activated natural clinoptilolite. *Environ. Eng. Manag. J* **2015**, *14*, 1705−1712.

(44) Mukherjee, S.; Weihermüller, L.; Tappe, W.; Hofmann, D.; Köppchen, S.; Laabs, V.; Vereecken, H.; Burauel, P. Sorption−desorption behaviour of bentazone, boscalid and pyrimethanil in biochar and digestate based soil mixtures for biopurification systems. *Sci. Total Environ.* **2016**, *559*, 63−73.

(45) Celebioglu, A.; Yildiz, Z. I.; Uyar, T. Thymol/cyclodextrin inclusion complex nanofibrous webs: Enhanced water solubility, high thermal stability and antioxidant property of thymol. *Food Res. Int.* **2018**, *106*, 280−290.

(46) Wang, J.; Cao, Y.; Sun, B.; Wang, C. Characterisation of inclusion complex of trans-ferulic acid and hydroxypropyl-*β*-cyclo-dextrin. *Food Chem.* **2011**, *124*, 1069−1075.

(47) Stražišar, M.; Andrenšek, S.; Šmidovnik, A. Effect of β-cyclodextrin on antioxidant activity of coumaric acids. *Food Chem.* **2008**, *110*, 636−642.

(48) Yuan, C.; Lu, Z.; Jin, Z. Characterization of an inclusion complex of ethyl benzoate with hydroxypropyl-β-cyclodextrin. *Food Chem.* **2014**, *152*, 140−145.

(49) Loftsson, T.; Hreinsdóttir, D.; Másson, M. Evaluation of cyclodextrin solubilization of drugs. *Int. J. Pharm.* **2005**, *302*, 18−28.

(50) Astray, G.; Gonzalez-Barreiro, C.; Mejuto, J. C.; Rial-Otero, R.; Simal-Gandara, J. A review on the use of cyclodextrins in foods. *Food Hydrocolloids* **2009**, *23*, 1631−1640.

(51) Mazzobre, M.; Elizalde, B.; dos Santos, C.; Cevallos, P. P.; Buera, M. Nanoencapsulation of food ingredients in cyclodextrins: Effect of water interactions and ligand structure. *Funct. Food Prod. Dev.* **2010**, *2*, 24.

(52) Tommasini, S.; Raneri, D.; Ficarra, R.; Calabrò, M. L.; Stancanelli, R.; Ficarra, P. Improvement in solubility and dissolution rate of flavonoids by complexation with β-cyclodextrin. *J. Pharm. Biomed. Anal.* **2004**, *35*, 379−387.

(53) DeLoid, G. M.; Wang, Y.; Kapronezai, K.; Lorente, L. R.; Zhang, R.; Pyrgiotakis, G.; Konduru, N. V.; Ericsson, M.; White, J. C.; De La Torre-Roche, R.; et al. An integrated methodology for assessing the impact of food matrix and gastrointestinal effects on the biokinetics and cellular toxicity of ingested engineered nanomaterials. *Part. Fibre Toxicol.* **2017**, *14*, 40.

(54) Euston, S. R.; Baird, W. G.; Campbell, L.; Kuhns, M. Competitive adsorption of dihydroxy and trihydroxy bile salts with whey protein and casein in oil-in-water emulsions. *Biomacromolecules* **2013**, *14*, 1850−1858.

(55) Galantini, L.; di Gregorio, M. C.; Gubitosi, M.; Travaglini, L.; Tato, J. V.; Jover, A.; Meijide, F.; Soto Tellini, V. H.; Pavel, N. V. Bile salts and derivatives: Rigid unconventional amphiphiles as dispersants, carriers and superstructure building blocks. *Curr. Opin. Colloid Interface Sci.* **2015**, *20*, 170−182.

(56) Small, D. M.; Cabral, D. J.; Cistola, D. P.; Parks, J. S.; Hamilton, J. A. The ionization behavior of fatty acids and bile acids in micelles and membranes. *Hepatology* **1984**, *4*, 77S−79S.

(57) Sarkar, A.; Ye, A.; Singh, H. On the role of bile salts in the digestion of emulsified lipids. *Food Hydrocolloids* **2016**, *60*, 77−84.

(58) Hansen, W. E. Effect of dietary fiber on pancreatic lipase activity in vitro. *Pancreas* **1987**, *2*, 195−198.

(59) Restiawaty, E.; Culsum, N. T. U.; Nishiyama, N.; Budhi, Y. W. Preparation, Characterization, and Surface Modification of Cellulose Nanocrystal from Lignocellulosic Biomass for Immobilized Lipase. *Fibers* **2022**, *10*, 33.

(60) Tiselius, A.; Henschen, G.; Svensson, H. Electrophoresis of pepsin. *Biochem. J.* **1938**, *32*, 1814−1818.

(61) Monopoli, M. P.; Åberg, C.; Salvati, A.; Dawson, K. A. Biomolecular coronas provide the biological identity of nanosized materials. *Nat. Nanotechnol.* **2012**, *7*, 779−786.

(62) Setyawati, M. I.; Zhao, Z.; Ng, K. W. Transformation of nanomaterials and its implications in gut nanotoxicology. *Small* **2020**, *16*, 2001246.

(63) Carta, G.; Murru, E.; Banni, S.; Manca, C. Palmitic acid: physiological role, metabolism and nutritional implications. *Front. Physiol.* **2017**, *8*, 902.

(64) Ye, Z.; Cao, C.; Liu, Y.; Cao, P.; Li, Q. Triglyceride structure modulates gastrointestinal digestion fates of lipids: A comparative study between typical edible oils and triglycerides using fully designed in vitro digestion model. *J. Agric. Food Chem.* **2018**, *66*, 6227−6238.

(65) Nepogodiev, S. A.; Stoddart, J. F. Cyclodextrin-based catenanes and rotaxanes. *Chem. Rev.* **1998**, *98*, 1959−1976.

(66) Rekharsky, M. V.; Inoue, Y. Complexation thermodynamics of cyclodextrins. *Chem. Rev.* **1998**, *98*, 1875−1918.

(67) Turnbull, W. B.; Daranas, A. H. On the value of c: can low affinity systems be studied by isothermal titration calorimetry? *J. Am. Chem. Soc.* **2003**, *125*, 14859−14866.

(68) Rispens, T.; Heer, P. O. d.; Derksen, N. I.; Wolbink, G.; van Schouwenburg, P. A.; Kruithof, S.; Aalberse, R. C. Nanomolar to sub-picomolar affinity measurements of antibody−antigen interactions and protein multimerizations: Fluorescence-assisted high-performance liquid chromatography. *Anal. Biochem.* **2013**, *437*, 118−122.

(69) Yuan, C.; Jin, Z.; Xu, X.; Zhuang, H.; Shen, W. Preparation and stability of the inclusion complex of astaxanthin with hydroxypropyl-β-cyclodextrin. *Food Chem.* **2008**, *109*, 264−268.

(70) Cao, X.; Zhang, T.; DeLoid, G. M.; Gaffrey, M. J.; Weitz, K. K.; Thrall, B. D.; Qian, W.-J.; Demokritou, P. Cytotoxicity and cellular proteome impact of cellulose nanocrystals using simulated digestion and an in vitro small intestinal epithelium cellular model. *NanoImpact* **2020**, *20*, 100269.

(71) DeLoid, G.; Cao, X.; Molina, R. M.; Silva, D. I.; Bhattacharya, K.; Ng, K. W.; Loo, J.; Brain, J.; Demokritou, P. Toxicological effects of ingested nanocellulose in in vitro intestinal epithelium and in vivo rat models. *Environ. Sci.: Nano* **2019**, *6*, 2105−2115.

(72) Khare, S.; DeLoid, G. M.; Molina, R. M.; Gokulan, K.; Couvillion, S. P.; Bloodsworth, K. J.; Eder, E. K.; Wong, A. R.; Hoyt, D. W.; Bramer, L. M.; et al. Effects of ingested nanocellulose on intestinal microbiota and homeostasis in Wistar Han rats. *NanoImpact* **2020**, *18*, 100216.

(73) Salari, M.; Bitounis, D.; Bhattacharya, K.; Pyrgiotakis, G.; Zhang, Z.; Purington, E.; Gramlich, W.; Grondin, Y.; Rogers, R.; Bousfield, D.; et al. Development & characterization of fluorescently tagged nanocellulose for nanotoxicological studies. *Environ. Sci.: Nano* **2019**, *6*, 1516−1526.